Synthesis and Photo-degradation of Polyphthalaldehydes with Oxime Ether Terminals

Journal of Photopolymer Science and Technology
Volume 33, Number 3 (2020) 269 – 278 ©2020SPST

Synthesis and Photo-degradation of Polyphthalaldehydes with Oxime Ether Terminals

Hirokazu Hayashi[1*], Hideki Tachi[2], and Kanji Suyama[3]**

[1] Research Division of Applied Material Chemistry,
[2] Research Division of Polymer Functional Materials,
Izumi Center, Osaka Research Institute of Industrial Science and Technology (ORIST),
7-1 Ayumino-2, Izumi, Osaka 594-1157, Japan
[3] Faculty of Liberal Arts and Sciences, Osaka Prefecture University,
1-1 Gakuencho, Nakaku, Sakai, Osaka 599-8531, Japan
**hayashi@tri-osaka.jp*
***suyama@las.osakafu-u.ac.jp*

The degradation and recycling of polymeric materials are growing public interests recently, and the molecular design of degradable polymers is highly important. Herein the syntheses and photochemical behavior of photolabile polyphthalaldehydes (PPAs) with oxime ether terminals are reported. *o*-Phthalaldehyde (*o*-PA) was polymerized with 1 or 2-acetonaphthone oxime as initiators in the presence of DBU at low temperature and terminated with acetic anhydride. The incorporation of naphthyl oxime ether units and acetyl terminals was confirmed by NMR, UV, and IR spectral measurements. The repeating units of obtained PPAs were about 100. When PPAs were irradiated with UV light (>310 nm) in $CHCl_3$, peaks due to *o*-PA appeared. On irradiation of PPA films, peaks appeared around 1775 cm^{-1} in IR spectra, suggesting the formation of phthalide which could be derived from photo-transformation of *o*-PA. These spectral changes clearly indicated the proceeding of photo-depolymerization of PPAs. In order to analyze the mechanical property changes of PPA films on irradiation, nanoindentation technique was attempted. It was found that reduced modulus of PPAs decreased on irradiation, which supported the photo-depolymerization as observed in spectral analyses.

Keywords: Photo-depolymerization, Self-immolative, Polyphthalaldehyde, Oxime ether, *E*/*Z* isomer, Nanoindentation technique

1. Introduction

The design of degradable polymeric materials on demand is highly desired. Several technologies including chemical, thermal, biological, electrical, photochemical and ultrasonic irradiation methods have been proposed for the degradation of the materials [1]. Among them, photochemical method is useful because of easy spatiotemporal control and small damage on many kinds of substrates [2,3]. These characteristics show that photochemical degradation is advantageous in the fields of chemical recycle, photoresists, and drug delivery systems.

It is also important to degrade networked polymers. The networked polymers are often used in components or parts of composite materials, and their excellent mechanical and thermally stability prevent from recycling them after use. Photo-triggered decrosslinking can be accomplished by releasing catalysts such as strong acids derived from photoacid generators (PAGs) [4]. The other method is to incorporate photolabile units into main-chain or linker units, although the units used in the crosslinkers were not so many except *o*-nitrobenzyl- [5–7] and coumarin-based [8,9] families. We have recently proposed oxime ester and carbamoyl ester moieties as the photolabile units [10-14] and succeeded in the decrease in peel strength of pressure-sensitive adhesives [11] and increase in the solubility of polyacrylates and polyurethanes in organic solvents on irradiation [10, 14]. However, in many cases, remarkable

Received March 16, 2020
Accepted March 29, 2020

mechanical changes were not observed.

On the other hand, end-to-end depolymerization (unzipping) can be achieved for some polymers such as polyphthalaldehydes (PPAs) [15]. As can be seen in Ito and Willson's pioneering work, the photo-induced depolymerization of PPAs has been reported [16]. Recently, PPAs attract much attention again as a candidate for self-immolative polymers [17,18].

In this article, we report the syntheses and photo-degradation of PPAs with oxime ether terminals as shown in Scheme 1.

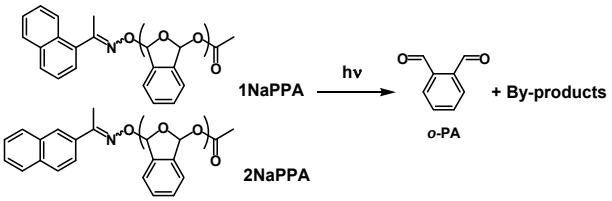

Scheme 1. Photo-degradation of PPAs with oxime ether terminals.

The degradation of PPAs can be possible by treating with acids [16]. ^{t}BuMe$_2$Si-capped PPAs could be depolymerized by adding F anion. Also, photochemical cleavage of *o*-nitrobenzyl-terminal led to the depolymerization of PPAs [19-21].

PPAs can be prepared by polymerization of *o*-phthalaldehyde (*o*-PA) with cationic catalysts, although obtained polymers are not linear but cyclic [15]. However, anionic polymerization gives linear PPAs [15]. Furthermore, it is easy to introduce various functional terminals into PPAs in the anionic mode.

We intended to introduce oxime ether units to PPA terminals because of their photo-degradable property and possibility to incorporate the units into cross-linked polymers by using multi-functional oximes. Therefore, we prepared PPAs by anionic polymerization.

It is known that major photoreactions of oxime ethers are *E*/*Z* isomerization and homolytic N–O cleavage [22-26]. The latter was utilized for syntheses of heterocyclic molecules [23,26]. The thermal [27] and hydrolytic stability [28] of oxime ethers were also reported.

Recently, nanoindentation technique that can evaluate mechanical properties of nanoscale surfaces has been used to investigate elastic modulus of polymers [29-35]. We have attempted to apply the nanoindentation technique to characterize the mechanical property changes of irradiated PPA films.

Herein, we investigate their photoreactivity in solution and solid state. In order to clarify the role of *E*/*Z* isomers of terminal oxime ether units in PPAs, acetonaphthone *O*-benzyloximes were prepared as model compounds and examined. Furthermore, the nanoindentation technique was utilized to evaluate the photo-depolymerization of PPA films.

2. Experimental

2.1. General

IR and UV spectra were recorded on Jasco FT-IR4200, and Shimadzu UV2400PC spectrometers, respectively. NMR spectra were measured by JEOL JNM-ECX400 and Bruker BioSpin Ascend 400 spectrometers, and obtained chemical shifts are expressed in ppm with tetramethylsilane as an internal standard. The micro-morphology of films was identified by a Hitachi High-technologies Regulus 8230 field emission scanning electron microscope (FE-SEM).

Simultaneous thermogravimetry-differential thermal analysis (TG/DTA) measurements were carried out using a Hitachi High-technologies STA7300 with a heating rate of 10 K min^{-1} under N_2. Melting points were measured with a Yanaco MPJ3 and uncorrected. Mass spectra were taken with a Thermo Scientific Q-Exactive by using electrospray ionization (ESI) in positive mode.

Number (M_n) and weight (M_w) average molecular weights of polymers were obtained by size exclusion chromatography (SEC) by using a Shimadzu LC-20AD liquid chromatography system (Kyoto, Japan) composed of two Shodex KF-805L polystyrene mixed gel columns, and a Wyatt differential refractometer Optilab T-rEX detector with THF eluent and polystyrene standards at 40 °C.

Commercially available reagents were used as received from Nacalai Tesuque (Kyoto, Japan) and TCI (Tokyo, Japan) unless otherwise noted.

2.2. Preparation of acetonaphthone oximes

In the flask, 6.01 g (35.3 mmol) of 1-acetonaphthone, 11.33 g (163 mmol) of hydroxylamine hydrochloride, 10 mL of EtOH, and 50 mL of pyridine were heated at 60 °C for 3 h. After removing the solvents under reduced pressure, resulting solid was washed with water thoroughly and recrystallized from methanol. Finally, 3.62 g (19.6 mmol) of 1-acetonaphthone oxime was obtained as colorless solid: Yield 55.5 %, mp = 138 – 139.5 °C (lit. [36] mp 134 – 141 °C, *E* form), ^{1}H NMR ($CDCl_3$): δ 8.01-8.03 (1H, m, aromatic), 7.86-7.89 (2H, m, aromatic), 7.44-7.53 (4H, m, aromatic), 2.38 (3H, s, CH_3). ^{13}C NMR ($CDCl_3$): δ 157.57,

135.46 133.81, 130.85, 129.15, 128.51, 126.27, 126.05, 125.92, 125.26, 125.22, 16.75.

According to similar method, 2-acetonaphthone oxime was obtained as 5.07 g (27.5 mmol) of colorless solid: Yield 77.9 %, mp = 132 – 137 °C (lit. [37] mp 146 – 147 °C), ^{1}H NMR ($CDCl_3$): δ 8.02 (1H, s, aromatic), 7.84-7.87 (2H, m, aromatic), 7.49-7.51 (4H, m, aromatic), 2.42 (3H, s, CH_3). ^{13}C NMR ($CDCl_3$): δ 156.03, 133.83 133.70, 133.11, 128.49, 128.18, 127.67, 126.69, 125.94, 123.29, 11.97.

2.3. Preparation of acetonaphthone *O*-benzyloximes

Acetonaphthone *O*-benzyloximes were obtained according to the method reported in literature [38].

1-Acetonaphthone *O*-benzyloxime: In a flask, 2.13 g (13.3 mmol) of benzylhydroxylamine hydrochloride, 2.26 g (13.3 mmol) of 1-acetonaphthone in 25 mL of pyridine were heated at 60 °C for 2.5 h. After removing the solvent under reduced pressure, 100 mL of ethyl acetate was added to the residue. Then the solution was washed with 0.12 N HCl twice and sat. $NaHCO_3$ aqueous solutions, respectively, and dried over sodium sulfate. After removing the solvent, 3.14 g colorless tar was obtained, which was purified with silica gel chromatography to afford two fractions. *E*/*Z* isomers of obtained products were determined according to literature [36].

(*E*)-1-Acetonaphthone *O*-benzyloxime (1NaBO-E): 2.20 g (7.97 mmol) of colorless tar (lit. [36] mp 36 – 37 °C), Yield 59.9 %, ^{1}H NMR ($CDCl_3$): δ 7.92-7.94 (1H, m, aromatic), 7.79-7.83 (2H, m, aromatic), 7.31-7.47 (9H, m, aromatic), 5.28 (2H, s, CH_2), 2.38 (3H, s, CH_3). ^{13}C NMR ($CDCl_3$): δ 156.92, 138.23 135.42, 133.85, 130.82, 129.02, 128.41, 128.40, 128.35, 128.25, 128.24, 128.23, 127.79, 126.42, 125.97, 125.92, 125.51, 125.13, 76.07, 17.52. UV ($CHCl_3$): λ_{max} 293.09 (molar extinction coefficient ε: 7.88×10^3 L·mol^{-1}·cm^{-1}), 288.8 (8.01×10^3), 283.7 (8.11×10^3), and 282.9 nm (7.31×10^3). High Resolution MS (ESI) *m/z*: [*M*+H$^+$] calcd for $C_{19}H_{18}NO$; 276.1336 found 276.1382.

(*Z*)-1-Acetonaphthone *O*-benzyloxime (1NaBO-Z): 0.80 (2.90 mmol) g of colorless solid: Yield 21.8 %, mp = 56.5 – 57.5 °C (lit. [36] mp 56 – 57 °C), ^{1}H NMR ($CDCl_3$): δ 7.84-7.80 (2H, m, aromatic), 7.58-7.60 (1H, m, aromatic), 7.40-7.50 (3H, m, aromatic), 7.21-7.28 (4H, m, aromatic), 7.16-7.18 (2H, m, aromatic), 5.01 (2H, s, CH_2), 2.24 (3H, s, CH_3). ^{13}C NMR ($CDCl_3$): δ 155.49, 138.37 134.95, 133.35, 128.90, 128.46, 128.35, 128.11, 128.09, 128.08, 127.93, 127.91, 127.43, 126.24, 126.06, 125.67, 125.26, 123.52, 75.54, 22.76. UV ($CHCl_3$): λ_{max} 313.7 (ε: 0.60×10^3 L·mol^{-1}·cm^{-1}), 292.9 (5.75×10^3), 282.9 (7.31×10^3), and 274.4 nm (6.02×10^3). High Resolution MS (ESI) *m/z*: [*M*+H$^+$] calcd for $C_{19}H_{18}NO$ 276.1336; found 276.1380.

Similarly, 2-acetonaphthone *O*-benzyloxime (2NaBO) was obtained as 0.84 g (3.04 mmol) of colorless solid after purification: Yield 22.9 %, mp = 99 – 99.5 °C, ^{1}H NMR ($CDCl_3$): δ 9.71 (3H, d *J* = 8.0 Hz, aromatic), 8.15 (3H, d, *J* = 7.2 Hz, aromatic), 7.45 (3H, m, aromatic), 7.26 (3H, s, aromatic), 6.35 (3H, s, =CH), 5.87 (3H, s, =CH), 2.21 (9H, s, CH_3). ^{13}C NMR ($CDCl_3$): δ 164.386, 158.254, 141.770, 140.225, 135.011, 132.716, 130.518, 129.583, 129.435, 128.594, 127.419, 19.028. UV ($CHCl_3$): λ_{max} 298.0 (ε: 1.48×10^4 L·mol^{-1}·cm^{-1}), 286.5 (1.70×10^4), and 277.6 nm (1.40×10^4). High Resolution MS (ESI) *m/z*: [*M*+H$^+$] calcd for $C_{19}H_{18}NO$ 276.1336; found 276.1383.

2.4. Polymerization

In a flask, 960 mg (7.16 mmol) of *o*-PA (SP grade for fluorometry, recrystallized, Nacalai) was dissolved in 2 mL of toluene and removed the solvent under reduced pressure. To the flask, 20 mL of CH_2Cl_2 (dehydrated grade, Nacalai, $H_2O < 50$ ppm) was added under Ar, and the flask was cooled to -80 °C in an aluminum block cryostat PSL-2500 A (EYELA, Tokyo, Japan). In other vial, 137 mg (0.90 mmol) of 1,8-diazabicyclo[5.4.0]undec-7-ene (DBU) and 166 mg (0.92 mmol) of 1-acetonaphthone oxime were dissolved in 5 mL of CH_2Cl_2. Then, 0.5 mL of the solution was taken out with a syringe and added to the flask dropwise over 20 s, and the mixture was kept stirring at -80 °C for 20 min.

The polymerization was quenched by dropping 1 mL of CH_2Cl_2 solution containing 17 μL of acetic anhydride (0.18 mmol) over 20 s, kept stirring at -80 °C for 10 min. The flask was taken out from the cryostat bath and stirred for 20 min at room temperature. Then, 5 mL of methanol was added to the flask and removed the solvent to obtain 902 mg of a white solid. The solid was reprecipitated three time from methanol after dissolving in CH_2Cl_2, and 403 mg of PPA with 1-acetonaphthone oxime terminal (1NaPPA) was obtained as colorless powder: ^{13}C NMR ($CDCl_3$): δ 138.87 138.75, 138.60, 133.77, 131.14, 129.74, 123.66, 123.22, 104.24, 103.73, 103.18, 102.91, 102.62.

Similarly, 429 mg of PPA with 2-acetonaphthone oxime terminal (2NaPPA) was obtained: ^{13}C NMR ($CDCl_3$): δ 138.87 138.73, 138.59, 133.77, 131.13, 129.73, 123.68, 123.21, 104.22, 103.72, 102.94, 102.61.

2.5. Photo-irradiation in solutions

Photo-irradiation was performed with a Hayashi Watch-Works LA410 Xe-Hg lamp (Tokyo, Japan). The light intensity was measured by an Orc UV-M03 illuminometer (Tokyo, Japan) and found to be 150 mW/cm^2 at 365 nm.

For the measurement of UV spectra, solutions were irradiated in a 1 × 1 cm quartz cuvette through 50 μm PET film in order to remove the influence of 254 nm light. For NMR spectral changes, solutions were irradiated in commercially available Pyrex 5 mm$^\phi$ NMR tubes.

2.6. Photo-irradiation in films

Polymer films were obtained by spin coating on silicon wafers or quartz plates from cyclohexanone or propylene glycol methyl ether acetate solutions and prebaked at 80 °C for 2 min on a hotplate in air. The average thickness of polymer films was ca. 0.4-0.5 μm, which was determined by the cross-sectional SEM images. The polymer films were overlapped with the PET film and were irradiated with the above light source.

2.7. Nanoindentation technique

Nanoindentation measurement was carried out using a Hysitron TI950 Triboindenter with a TI-0039 Berkovich diamond tip (half angle 65.3º, total induced angle 142.3º) at room temperature. Prior to measurement, the tip area function was calibrated using a fused quartz standard sample. The trapezoidal loading pattern was carried out (loading segment: 5 s, load holding segment: 5 s, unloading segment: 5 s). The maximum applied load was 80 μN in a load-control mode. The thermal drift was kept below 0.3 nm/s. Hardness (H) and reduced modulus (Young's modulus E_r) were calculated using the Oliver and Pharr method [29] using Eqs. (1) and (2),

$$H = P_{max}/A \quad (1)$$

$$E_r = S\sqrt{\pi}/2\sqrt{A} \quad (2)$$

where P_{max} is maximum load, A is an area of contact, and S is the contact stiffness. S is obtained from the slope (dP/dd) of the load-displacement curve at P_{max}, where P is derivative load and d is impression depth. E_r is also defined as Eq. (3),

$$1/E_r = (1-\nu_s{}^2)/E_s + (1-\nu_i{}^2)/E_i \quad (3)$$

where ν_i is Poisson's ratio for the diamond tip (0.07), ν_s is Poisson's ratio of the sample, E_s is elastic modulus of the sample, E_i is elastic modulus of diamond tip (1140 GPa). In this study, these plots were averaged from 7 indent runs.

3. Results and discussion

3.1. Syntheses and characteristics of PPAs with oxime ether terminals

PPAs were prepared by anionic polymerization of *o*-PA using oximes as initiators and DBU as a catalyst. We prepared oximes from corresponding ketones and hydroxylamine hydrochloride. In case of 1-acetonaphthone oxime, the isolation and characterization of *E*/*Z* isomers have been established [39], and our oxime seems to be *E* form from a peak due to CH_3 at 2.38 ppm in the ^{1}H NMR spectrum. Unfortunately, we could not find such information on 2-acetonaphthone oxime in literatures.

The characteristics of obtained polymers are shown in Table1. The monomer conversions after purification were not high, probably due to rough polymerization atmosphere and not-purified reagents. From M_n values, the repeating units of 1NaPPA and 2NaPPA are estimated to be 85 and 112, respectively. Polydispersity index (PDI) (M_w/M_n) of 1NaPPA and 2NaPPA were 1.37, 1.26, showing lower PDI, respectively.

Table 1. Characteristics of PPAs.

PPA	Conv. (%)[a]	M_n[b]	M_w[b]	T_d (ºC)[c]
1NaPPA	42.0	11600	15900	221
2NaPPA	44.6	15200	19100	229

a) After reprecipitation.
b) From SEC with polystyrene standards and THF eluent.
c) From TG profiles.

Figure 1 shows IR spectra of 1NaPPA and 2NaPPA films, where peaks around 1730 cm^{-1} are observed. These peaks are assignable to acetyl units, showing the polymer chains were end-capped with acetyl units. In ^{1}H NMR spectra of both PPAs, small peaks at 2.1 and 2.4 ppm are observed along with broad bands (6.5-7.7 ppm) due to aromatic and methine protons in main-chains as shown in Fig. 2. Peaks due to CH_3 units in 1NaBO-Z and 1NaBO-E

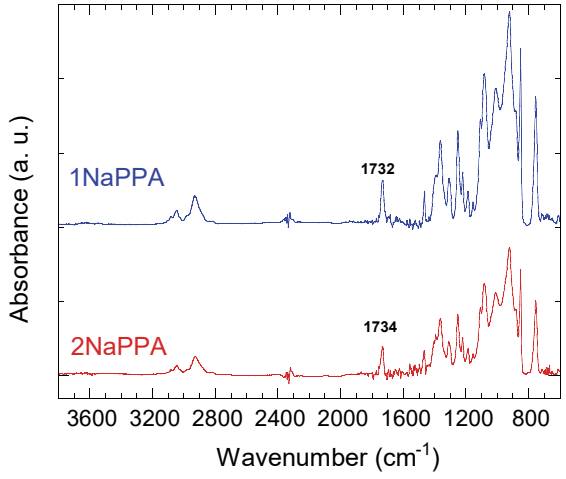

Fig. 1. IR spectra of PPA films.

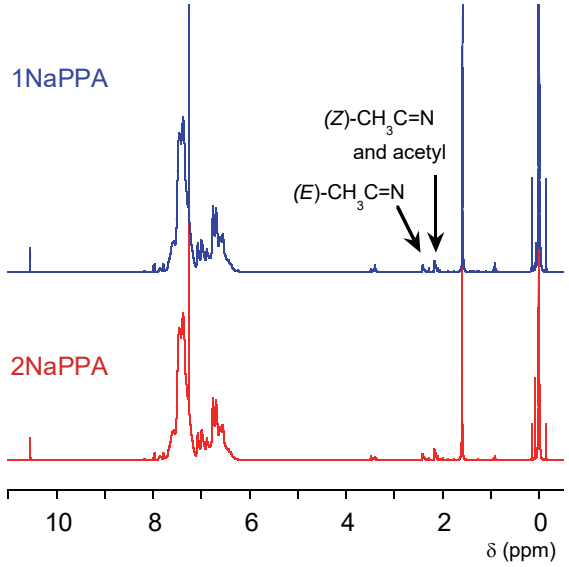

Fig. 2. ^{1}H NMR spectra of PPAs in $CDCl_3$.

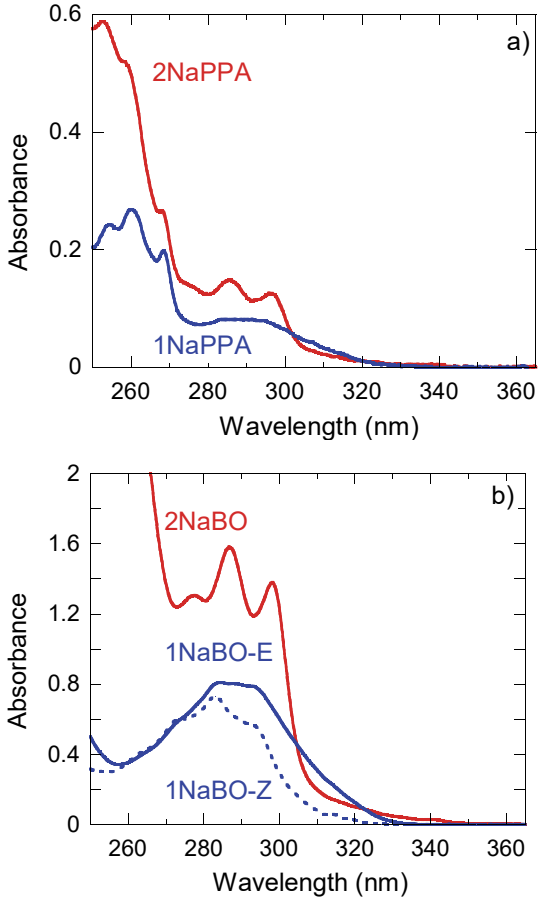

Fig. 3. UV spectra of a) PPAs in $CHCl_3$: 2.5 mg/25 mL, respectively, and b) 0.1 mM molecular oxime ethers in $CHCl_3$.

located at 2.2 and 2.4 ppm, respectively, and that due to acetyl unit were reported to be at 2.1 ppm [40]. Therefore, peaks at 2.1 ppm of 1NaPPA would be assigned to CH_3 units of both oxime ether (*Z* form) and acetyl units, and that at 2.4 ppm was assigned to oxime ether (*E* form). Similar small peaks were also observed in 2NaPPA spectrum.

Figure 3 shows UV spectra of PPAs and molecular oxime ethers. The spectrum of 1NaPPA (Fig. 3a) shows a broad band at 280-300 nm which is identical to that of 1NaBO-E as model compound (Fig. 3b). Considering that 1-acetonaphtone oxime that we used as an initiator seems almost *E* form, the stereoisomer would be kept even after incorporation into polymer terminal. 2NaPPA (Fig. 3a) shows characteristic trimodal peaks at 277, 286, and 298 nm which is also found in 2NaBO (Fig. 3b). These results clearly indicate that naphthyl units were incorporated in polymer terminals.

From TG/DTA profiles (Fig. 4), it is found that T_ds were 221 °C for 1NaPPA and 229 °C for 2NaPPA, showing that they were stable up to 200 °C. T_gs of PPAs were not observed clearly. These properties are often observed for PPAs prepared in anionic mode [15]. Slight decreases of TG profiles started at 185 and 168 °C for 1NaPPA and 2NaPPA, respectively, which was also observed for PPAs initiated with *n*-BuLi in strictly dehydrated atmosphere previously [16].

3.2. Photochemical behavior of PPAs in solutions

^{1}H NMR spectral changes of PPAs in $CDCl_3$ on irradiation were monitored to analyze their photo-

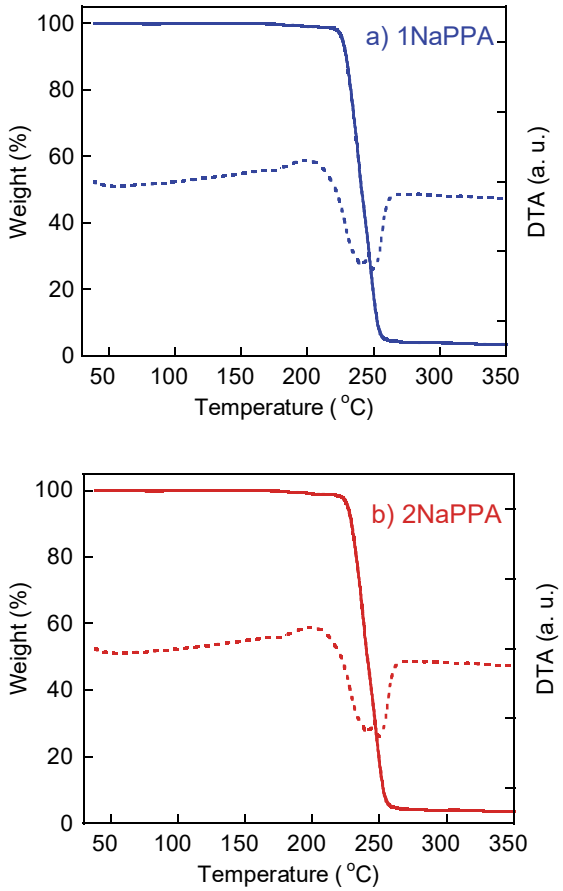

Fig. 4. TG (solid) and DTA (dashed) profiles of a) 1NaPPA and b) 2NaPPA.

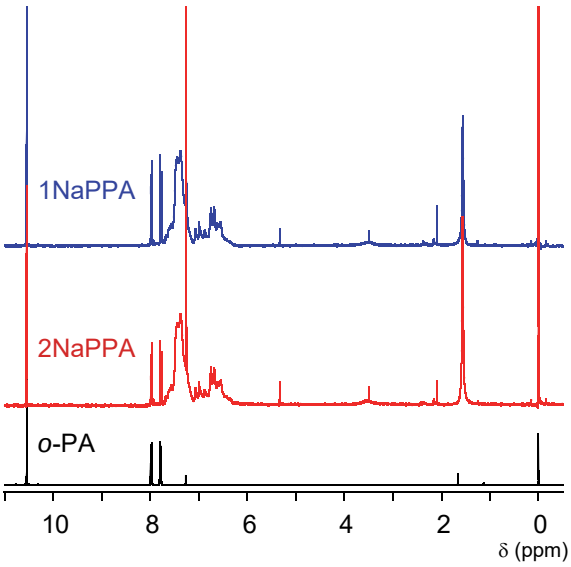

Fig. 5. ^{1}H NMR spectra of PPAs after irradiation for 10 min and *o*-PA in $CDCl_3$.

reaction. As shown in Fig. 5, the peaks due to polymer main-chains decreased along with the

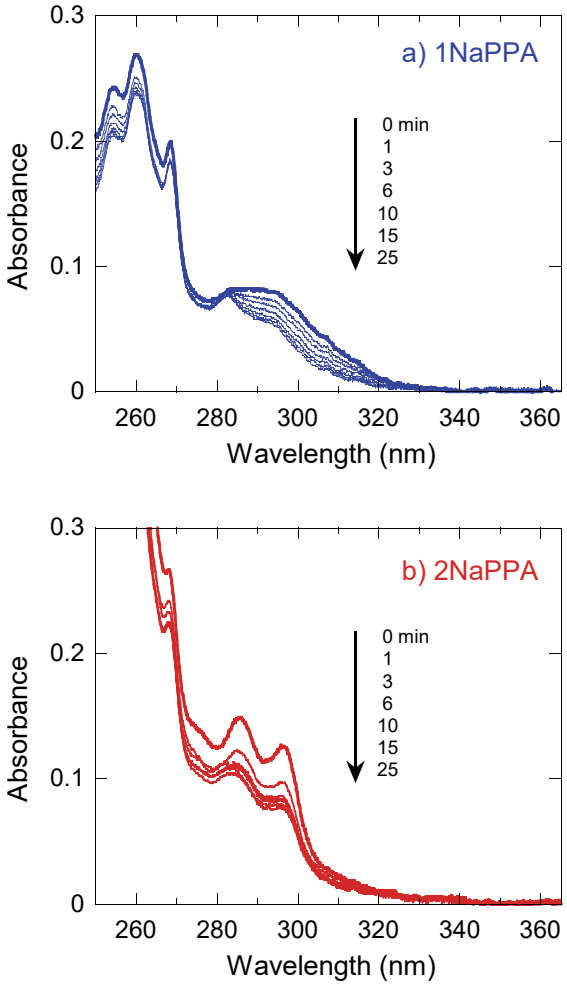

Fig. 6. UV spectral changes of $CHCl_3$ solutions (2.5 mg/25 mL) of a) 1NaPPA and b) 2NaPPA on irradiation. Irradiation: 0, 1, 3, 6 10, 15, 25 min.

appearance of sharp peaks at 7.8, 8.0, and 10.5 assignable to *o*-PA monomer for both polymers after irradiation for 10 min. Furthermore, new peak appeared at 5.3 ppm probably due to phthalide. Comparing with the spectra before irradiation (Fig. 2), these spectra clearly indicate the proceeding of photo-depolymerization.

Figures 6 and 7 show the UV spectral changes of PPAs and molecular oxime ethers in $CHCl_3$. For 1NaPPA (Fig. 6a), the band around 290-320 nm decreased, although the peak at 280 nm showed little changes. This behavior is similar to that of 1NaBO-E (Fig. 7a) in which the shoulder at 292 nm disappeared, remaining a peak at 283 nm (Fig. 6a), and the final spectrum was identical to that of 1NaBO-Z (Fig. 7b) which showed little changes. These results suggest that photo-isomerization from *E* to *Z* proceeded in 1NaPPA. These behaviors are consistent with the results of tetrazoline oxime ethers in literature [41], where *E* to *Z* photo-

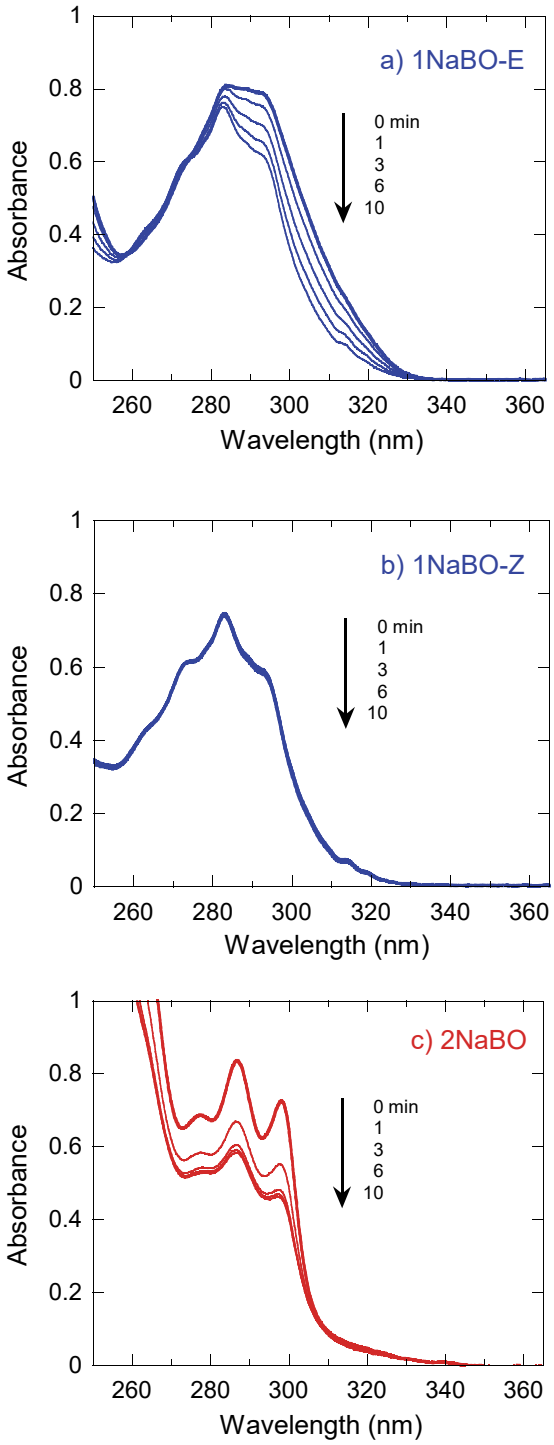

Fig. 7. UV spectral changes of a) 0.1 mM 1NaBO-E, b) 0.1 mM 1NaBO-Z, and c) 0.05 mM 2NaBO solution in $CHCl_3$ on irradiation. Irradiation: 0, 1, 3, 6, 10 min.

isomerization and subsequent photolysis of *Z* isomer proceeded on irradiation. These results suggest that the photo-isomerization and photo-depolymerization proceeded on irradiation of 1NaPPA film.

The UV spectral changes of 2NaPPA in $CHCl_3$ (Fig. 6b) was similar to that of 2NaBO (Fig. 7c), both show the gradual decrease of the band in the region of 270-310 nm, showing similar photoreaction proceeded, in spite that it was unclear whether photo-isomerization occurred or not.

3.3. Photochemical behavior of PPAs in films

The UV spectral changes of PPA films on irradiation were similar to that of PPA solutions, where both show the gradual decrease of the band around 290 nm (Fig. 8). These results suggest the photo-depolymerization proceeded in the films.

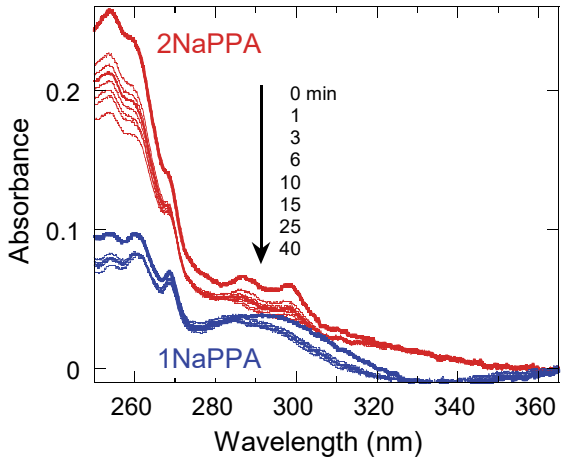

Fig. 8. UV spectral changes of PPA films on irradiation. Irradiation: 0, 1, 3, 6 10, 15, 25, 40 min.

The IR spectral changes of PPA films on irradiation are shown in Fig. 9, where peaks around 1775 cm^{-1} appeared in both films. The authentic samples of *o*-PA and phthalide have C=O stretching bands at 1687 and 1767 cm^{-1}, respectively. It is well-known that *o*-PA isomerizes to phthalide in many solutions on irradiation [42]. Along with the results of NMR spectral changes (Fig. 5), we conclude that the depolymerization of PPAs led to the formation of *o*-PA which was further photo-transformed into phthalide as shown in Scheme 2.

3.4. Nanoindentation measurement of PPA films

We measured mechanical property changes of PPA films on irradiation by means of nanoindentation technique which can estimate nano-mechanical properties of materials surface. Generally, this system gives hardness (*H*) and reduced modulus (Young's modulus E_r) of the outermost surfaces in films by measuring impression depth and load changes when diamond tip is impressed to the surface. Figure 10 shows schematic illustration and typical unloading slopes

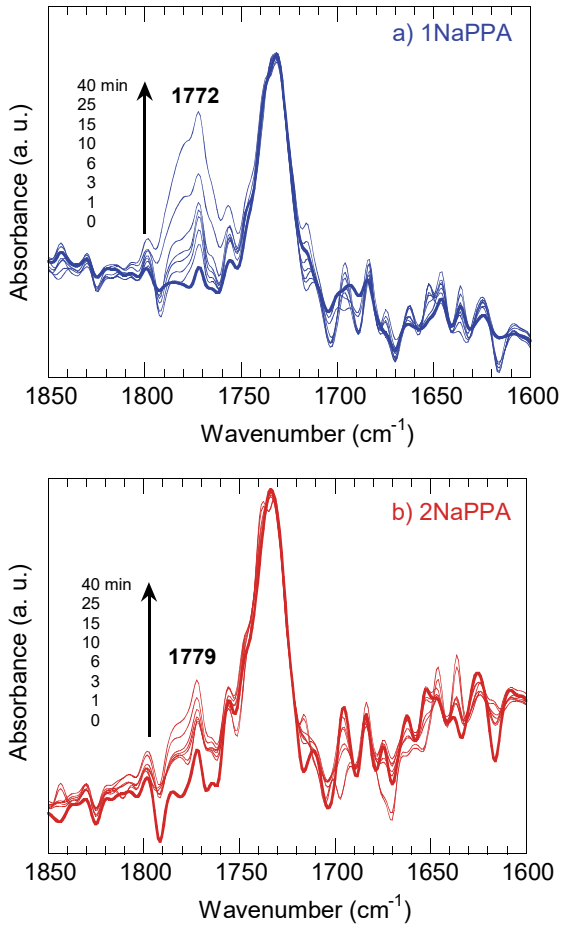

Fig. 9. IR spectral changes of a) 1NaPPA, and b) 2NaPPA on irradiation. Irradiation: 0, 1, 3, 6, 10, 15, 25, 40 min.

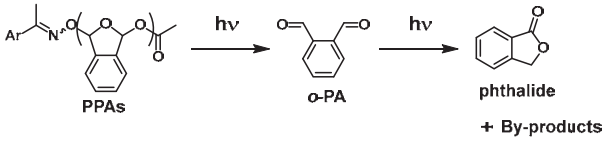

Scheme 2. Plausible photoreaction of PPAs with oxime ether terminals.

for PPA films in a load-control mode. The impression depth of both PPA films before irradiation were almost identical. However, it was found that the impression depth after irradiation of 1NaPPA film was greater than that of 2NaPPA.

Table 2 summarizes H and E_r for PPA films before and after irradiation for 20 min. Both parameters of PPAs before irradiation were almost the same. For 1NaPPA and 2NaPPA films after irradiation, E_r values reduced by 55% and 40%, respectively, showing that 1NaPPA film became

Table 2. H and E_r of PPA films.

PPA	E_r (GPa)[a]		H (GPa)[a]	
	0 min	20 min	0 min	20 min
1NaPPA	27.74	12.29	0.67	0.50
2NaPPA	27.12	16.48	0.63	0.55

a) Calculated using the Oliver and Pharr method [29]. Averaged values of 7 indent runs.

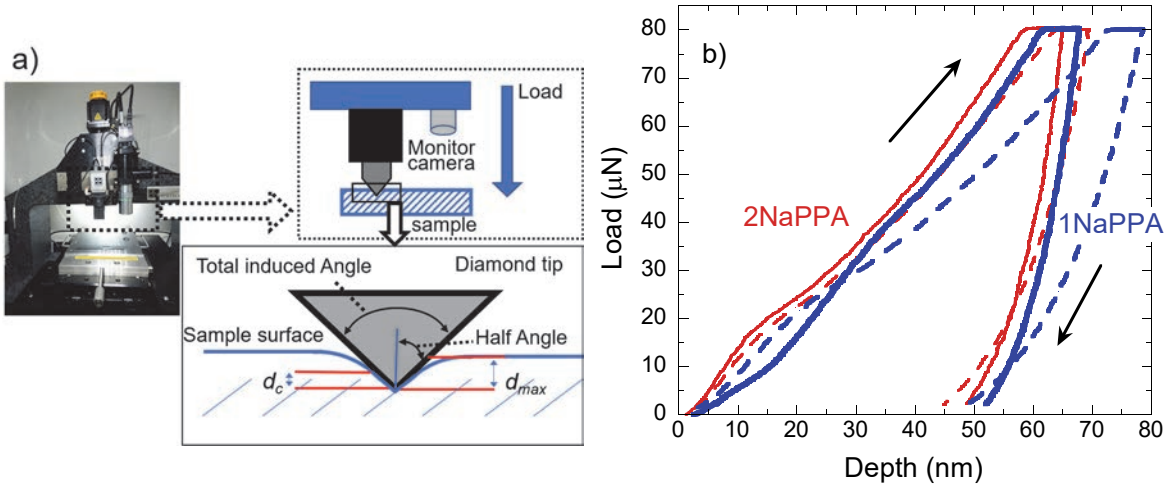

Fig. 10. Nanoindentation system in this study. a) Schematic illustration and b) typical unloading slopes for PPA films before (solid) and after (dashed) irradiation for 20 min. Data were obtained in load holding mode with maximum applied load of 80 μN. d_{max}: maximum impression depth, d_c: contact depth.

more elastic than 2NaPPA film. The values of *H* slightly decreased on irradiation. This might be explained that resulting *o*-PA monomer and phthalide are hard enough at room temperature, and thus photo-depolymerization was not reflected the changes of the surface hardness. These results are in good agreement with those of spectral changes on irradiation. Nanoindentation technique is very useful for research of nanoscale surface state such as photochemical reaction on polymer films.

4. Conclusion

We have synthesized PPAs with oxime ether terminals and their photoreactions have been investigated. PPAs with low PDI were successfully obtained by using acetonaphthone oximes and DBU. The incorporation of oxime ether and acetyl terminals were confirmed by NMR, IR, and UV spectra.

On UV irradiation of PPAs in $CHCl_3$ and in films, the proceeding of the depolymerization was confirmed by detecting the formation of *o*-PA and phthalide in NMR and IR spectral measurements. The photochemical behaviors of 1NaPPA including *E*/*Z* photo-isomerization were consistent with those observed for corresponding molecular oxime ethers.

Nanoindentation measurement clarified that the decrease in E_r for both PPA films on irradiation, showing the films became elastic. These results indicate that the nanoindentation technique is potential candidate for the evaluation of photoreactive films.

Acknowledgement

This work was supported by Masuya Memorial Basic Research Foundation and Ogasawara Foundation. The authors also thank to Dr. Junpei Kobata and Dr. Yohtaro Inoue, both of ORIST, for nanoindentation and NMR analyses, respectively, and to Prof. Haruyuki Okamura of Osaka Prefecture University for SEC analysis.

References

1. D. J. Fortman, J. P. Brutman, G. X. De Hoe, R. L. Snyder, W. R. Dichtel, and M. A. Hillmyer, *ACS Sustainable Chem. Eng*., **6** (2018) 11145.
2. E. Blasco, M. Wegener, and C. Barner-Kowollik, *Adv. Mater.*, **29** (2017) 1604005.
3. T. Chen, H. Wang, Y. Chu, C. Boyer, J. Liu, and J. Xu, *ChemPhotoChem.*, **3** (2019) 1059.
4. M. Shirai, *Polym. J.*, **46** (2014) 859.
5. A. M. Kloxin, A. M. Kasko, C. N. Salinas, and K. S. Anseth, *Science*, **324** (2009) 59.
6. D. Klinger and K. Landfester, *Macromolecules*, **44** (2011) 9758.
7. S. Bian, J. Zheng, and W. Yang, *J. Polym. Sci., Part A: Polym.Chem.*, **52** (2014) 1676.
8. Q. Huang, C. Bao, W. Ji, Q. Wang, and L. Zhu, *J. Mater. Chem*., **22** (2012) 18275.
9. M. A. Azagarsamy, D. D. McKinnon, D. L. Alge, and K. S. Anseth, *ACS Macro Lett*., **3** (2014) 515.
10. K. Suyama and H. Tachi, *RSC Adv*., **5** (2015) 31506.
11. K. Suyama and H. Tachi, *J. Photopolym. Sci. Technol*., **28** (2015) 45.
12. K. Suyama and H. Tachi, *Prog. Org. Coat*., **100** (2016) 94.
13. H. Tachi and K. Suyama, *J. Photopolym. Sci. Technol*., **29** (2016) 139.
14. K. Suyama and H. Tachi, *J. Photopolym. Sci. Technol*., **30** (2017) 247.
15. F. Wang and C. E. Diesendruck, *Macromol. Rapid Commun.,* **39** (2018) 1700519.
16. H. Ito and C. G. Willson, *Polym. Eng. Sci*., **23** (1983) 1012.
17. R. E. Yardley, A. R. Kenaree, and E. R. Gillies, *Macromolecules*, **52** (2019) 6342.
18. J. P. Lutz, O. Davydovich, M. D. Hannigan, J. S. Moore, P. M. Zimmerman, and A. J. McNeil, *J. Am. Chem. Soc*., **141** (2019) 14544.
19. A. M. Dilauro, H. Zhang, M. S. Baker, F. Wong, A. Sen, and S. T. Phillips, *Macromolecules*, **46** (2013) 7257.
20. S. T. Phillips, J. S. Robbins, A. M. Dilauro, and M. G. Olah, *J. Appl. Polym. Sci*., (2014) 40992.
21. A. M. DiLauro, J. S. Robbins, and S. T. Phillips, *Macromolecules*, **46** (2013) 2963.
22. A. Padwa and F. Albrecht, *Tetrahedoron Lett*., **1974** (1974) 1083.
23. A. J. McCarroll and J. C. Walton, *J. Chem. Soc., Perkin Trans. 2*, **2000** (2000) 1868.
24. J. C. Walton, *Molecules*, **21** (2016) 63.
25. H. J. Peter de Lijser and C.-K. Tsai, *J. Org. Chem*., **69** (2004) 3057.
26. K. Usami, E. Yamaguchi, N. Tada, and A. Itoh, *Org. Lett*., **20** (2018) 5714.
27. J. A. Blake, K. U. Ingold, S. Lin, P. Mulder, D. A. Pratt, B. Sheeller, and J. C. Walton, *Org. Biomol. Chem*., **2** (2004) 415.
28. J. Kalia and R. T. Raines, *Angew. Chem. Int. Ed.*, **47** (2008) 7523.
29. W. C. Oliver and G. M. Pharr, *J. Mater. Res.*, **7** (1992) 1564.
30. D. Tranchida, S. Piccarolo, J. Loos, and A. Alexeev, *Macromolecules*, **40** (2007) 1259.

31. S. Chattaraj, P. Pant, and H. Nanavati, *Polymer*, **144** (2018) 128.
32. T. Pertin, G. Minatchy, M. Adoue, A. Flory, and L. Romana, *Polym. Test.*, **81** (2020) 106194.
33. M. M. Zieger, P. Müller, E. Blasco, C. Petit, V. Hahn, L. Michalek, H. Mutlu, M. Wegener, and C. Barner-Kowollik, *Adv. Funct. Mater.*, **28** (2018) 1801405.
34. M. Rikkou-Kalourkoti, E. N. Kitiri, C. S. Patrickios, E. Leontidis, M. Constantinou, G. Constantinides, X. Zhang, and C. M. Papadakis, *Macromolecules*, **49** (2016) 1731.
35. P. Bandyopadhyay, M. Dwivedi, H. Krishnaswamy, and P. Ghosh, *Polymer*, **191** (2020) 122274.
36. W. Ou, S. Espinosa, H. J. Meléndez, S. M. Farré, J. L. Alvarez, V. Torres, I. Martínez, K. M. Santiago, and M. Ortiz-Marciales, *J. Org. Chem.*, **78** (2013) 5314.
37. H. Zhao, C. P. Vandenbossche, S. G. Koenig, S. P. Singh, and R. P. Bakale, *Org. Lett.*, **10** (2008) 505.
38. J. B. Summers Jr., A. O. Stewart, and D. W. Brooks, Eur. Patent EP 0292699 A2 (1987).
39. A. S. C. Chan, C.-C. Chen, C.-W. Lin, Y.-C. Lin, M.-C. Cheng, and S.-M. Peng, *J. Chem. Soc., Chem. Commun.*, **1995** (1995) 1767.
40. S. Lee, P. S. J. Kaib, and B. List, *J. Am. Chem. Soc.*, **139** (2017) 2156.
41. M. Fréneau, P. de S. Claire, N. Hoffmann, J.-P. Vors, J. Geist, M. Euvrard, and C. Richard, *RSC Adv.*, **6** (2016) 5512.
42. M. D. Tzirakis, N. G. Malliaros, and M. Orfanopoulos, *Eur. J. Org. Chem.*, **2019** (2019) 6961.